Available online at www.sciencedirect.com
ScienceDirect
Journal of the European Ceramic Society 27 (2007) 2623–2627
www.elsevier.com/locate/jeurceramsoc

Influence of thickness on the constrained sintering of alumina films

Olivier Guillon *, Stefanie Krauß, Jürgen Rödel

Darmstadt University of Technology, Department of Materials Science, Petersenstr. 23, D-64287 Darmstadt, Germany

Received 19 August 2006; received in revised form 4 October 2006; accepted 16 October 2006
Available online 27 November 2006

Abstract

Alumina films prepared by tape casting were sintered freely and under geometrical constraint at 1350 °C. The effect of film thickness on sintering kinetics and microstructure development was investigated. A decrease in film thickness in the constrained case leads to enhanced retardation of densification and increased orientation of anisometric pores.

Keywords: Films; Al_2O_3; Sintering; Anisotropy

1. Introduction

High hardness and inertness of ceramic materials make thin coatings interesting for protection of substrate materials against corrosion, oxidation and wear. However, achievement of defect-free fully sintered ceramic films is still a challenge if no accommodating viscous flow is present. All densification takes place in the thickness direction and an in-plane biaxial tensile stress develops which retards overall densification and may induce defects such as cracks or delamination.[1] Still, only limited research on the influence of the geometrical constraint on the sintering kinetics and microstructure evolution of such layers has been done. Garino and Bowen[2] proposed that films of particles consolidated by solid-state sintering behave differently from films that sinter by viscous flow, and suggested that microstructural anisotropy arises in those films. Investigating gold circuit pastes, Choe et al.[3] could not differentiate free from constrained sintered films by means of grain size measurements, so that the observed densification retardation could not be explained by the grain coarsening argument. Our recent work[4] revealed, however, that 20 μm thick alumina films produced by dip coating show a continuous development of anisotropy in the thickness plane. Pores become more anisometric with the long axis aligned along the thickness direction (normal to the plane of the film). No influence of the constraining conditions was observed on the mean grain size, but grains tend to become more equiaxed in the constrained plane, presumably due to the biaxial tensile stress state.

In the sense of the continuum mechanical description, a thin film is characterised by a negligible thickness compared with the two other lateral dimensions.[5–7] Under this assumption, the layer should be homogeneous across its thickness and the in-plane tensile stresses constant whatever the distance from the substrate may be. However, it is important to verify that real films meet these assumptions. The goal of the present study is to manufacture ceramic films of different thicknesses on a stiff substrate, to measure their shrinkage behaviour, to quantify any anisotropy development in the microstructure and to assess any gradients through the thickness.

2. Experimental procedure

Tape casting is a very successful method to process large area homogeneous ceramic films.[8] For the slurry processing, dried alumina powder (TM-DAR, 99.99% Al_2O_3) was suspended in a mixture of organic solvent and dispersant and treated ultrasonically for 15 min.[9] A milling step with YSZ-milling balls for 24 h was done in order to obtain the most homogeneous dispersion. Subsequently butylbenzylphthalate as a plasticizer and polyvinylbutyral as a binder were added into the suspension[10,11] and a second dispersion milling step was performed for 12 h with YSZ-milling balls. Table 1 shows a detailed description of the ingredients and amounts used for the slip preparation. Slurry viscosity was measured in a rotational viscometer with coaxial cylinder (Rheolab MC1, Paar Physica, Stuttgart, Germany). The suspension showed pseudoplastic behaviour and its viscosity

* Corresponding author. Tel.: +49 6151 165542; fax: +49 6151 166314.
E-mail address: guillon@ceramics.tu-darmstadt.de (O. Guillon).

0955-2219/$ – see front matter © 2006 Elsevier Ltd. All rights reserved.
doi:10.1016/j.jeurceramsoc.2006.10.007

Table 1
Slip composition

Component	Description	Amount (wt.%)	Amount (vol.%)
Solvent	Toluene/ethanol (azeotropic)	35.44	65.81
Dispersant	Menhaden fish oil, DEFLOC® Z3, Reichhold Inc., USA	0.96	1.47
Ceramic powder	α-Al_2O_3, TM-DAR, TAIMEI Chemicals, Japan, $d_{50} = 0.15\,\mu m$	55.50	21.09
Binder	Polyvinylbutyral (PVB), Mowital SB45 H, Kuraray-KSE, Germany	4.17	6.31
Plasticizer	Butyl benzyl phtalate (BBP), SANTICIZER® 160, Ferro, USA	3.93	5.32

decreased with increasing shear rate between 1.6 and 1.1 Pa s, which is well adapted to the processing method chosen. The produced slurry was tape cast with a blade height of 0.2 mm and a casting velocity of 1.6 cm/s onto either a fine-grained, high-purity alumina plate (CeramTec, Germany, R710, 0.1 μm grain size, 99.6% Al_2O_3, 0.63 mm thickness, surface roughness <0.1 μm) or onto a siliconized PETP carrier film. The tapes on the polymer carrier film were removed and cut into square pieces of 50 mm × 50 mm. The reference axes are: x for the tape casting direction, y the transverse and z the thickness direction. Multilayers of 10 tapes without substrate were used for free sintering experiments. In order to investigate the sintering behaviour of alumina films on rigid substrates as a function of thickness, samples with 1 and 3 layers (corresponding to a total thickness of about 50 and 150 μm, respectively) onto alumina plate were fabricated. The tape cast films were stacked together (with special care to align all layers along the casting direction) and laminated under uniaxial pressure with a closed die press (Dr. Collin). All specimens were laminated under the same conditions at 60 MPa and 80 °C for 20 min.

Based on the pyrolysis behaviour of the organic additives determined by thermal gravimetric analysis, the sintering program was defined as follows: the samples were heated up to 550 °C with a slow heating rate (1 °C/min) in order to guarantee the complete binder burnout without sample cracking and then heated with a heating rate of 20 °C/min up to 1350 °C and sintered for 4 h. For the free samples the shrinkage measurement in all directions took place in a horizontal pushrod dilatometer (DIL 402E, Netzsch, Germany). For the constrained specimens, sintering was carried out in a custom-designed optical dilatometer.[12] A high resolution vertical laser scanner measures the shrinkage in the direction perpendicular to the layer plane (z-direction), which is amplified mechanically by a rocking arm. In both configurations, a thermocouple was placed near the specimen for a precise temperature control.

The density before sintering was determined geometrically, whereas the density of the fired samples and the grain size were determined by micrograph analysis. For this purpose, samples were embedded in resin and their cross-sections (in YZ plane) polished. After a thermal etching at 1250 °C for 20 min, 9 micrographs of each sample were generated in a High Resolution Scanning Electron Microscope (XL30FEG, Phillips, Germany).

Porosity analysis taking into account more than 600 pores was performed with ImageJ software (NIH, USA). Micrographs were modified in the following way[4]: contrast enhancement, background subtracting, median filtering and thresholding in order to obtain suitable binary images. Some pores had to be manually handled to avoid errors in pore areas. Then an ellipse of equivalent area was generated for each pore and its angle with a horizontal line automatically determined. Grain size measurements were accomplished using the linear intercept method with a correction factor of 1.56 (Lince software, S. L. dos Santos e Lucato, TU Darmstadt, FB Materials Science, Ceramics Group). A set of orthogonally displayed lines (according to the global coordinate system) allowed determination of a horizontal and vertical characteristic grain length.

3. Results and discussion

3.1. Macroscopic densification behaviour

Fig. 1 provides the strains measured for freely sintered and constrained films as a function of isothermal time. For the case of free sintering, the strain curves measured along the casting direction and normal to it are similar (the ratio $\varepsilon_x/\varepsilon_y$ decreases continuously with time from 1.11 to about 1.03). The shrinkage in the thickness direction ε_z is less and the ratio $\varepsilon_x/\varepsilon_z$ increases from 1 at the beginning up to 1.19. The tape casting process is known to induce particle orientation and noticeable anisotropic shrinkage, if shear rate and solid content are high and ceramic particles are anisometric.[13] This effect can be reduced by the lamination conditions which modify the shrinkage behaviour of tape cast multilayered ceramics.[14] The use of a closed die press can lead to matter reorganisation and almost isotropic shrinkage during sintering.

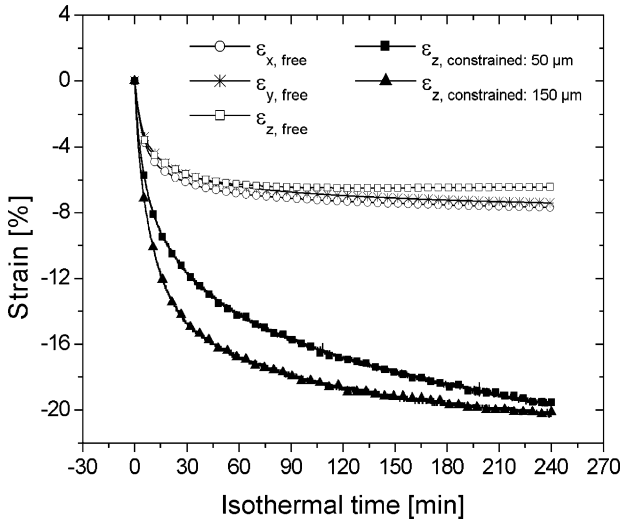

Fig. 1. Strains of free and constrained films as a function of isothermal time.

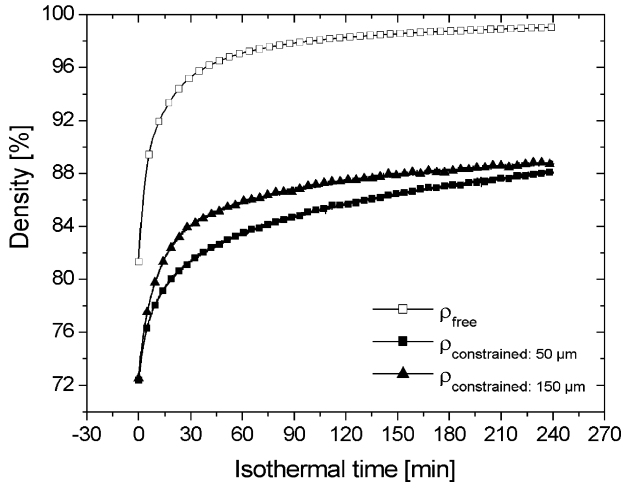

Fig. 2. Density of free and constrained films as a function of isothermal time.

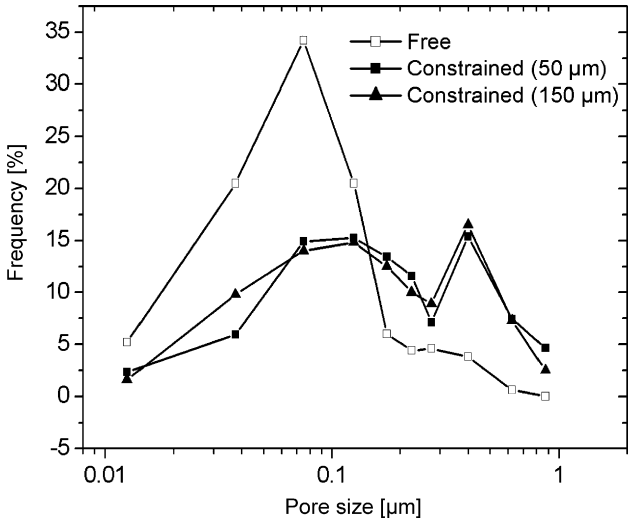

Fig. 3. Pore size distribution at 90% density (averaged through the whole thickness).

The strain ε_z for constrained films is found to be almost three times higher than for freely sintered ones after 4 h of isothermal time. This result is expected as all the densification takes place along this direction.[5] Strain rates (equal to the densification rate for the constrained films) are affected by the film thickness: the 150 μm thick coating sinters more rapidly than the 50 μm thick one.

In Fig. 2, film density is plotted as a function of isothermal time. Green density is about 55% for all specimens. After 4 h of isothermal time, the freely sintered specimens are almost fully densified (99.0% of density). Constrained films shrink more rapidly in the unconstrained direction in comparison with freely sintered specimens, but not at all in the other directions, so that global densification is retarded. Initial density at 1350 °C is only 72% independent of film thickness, whereas it is almost 82% for the free film. As already observed in Fig. 1, densification is more retarded for the thinner film, which seems to be more constrained than the thicker one. After 4 h of sintering, final densities are, however, close to each other (88.0 and 88.7%, respectively). No delamination or cracking was observed, assuring optimal constraining conditions.

3.2. Analysis of microstructure

First of all, mean porosity parameters were evaluated from micrographs taken from the whole cross-section. Pore size distribution is influenced by the sintering conditions, as shown in Fig. 3 for a density of 90%. The distribution is monomodal for the freely sintered film, with a large peak centred at 0.075 μm. More big pores are left in the constrained specimens, for which the pore size distribution is bimodal, showing maximal frequencies for 0.1 and 0.5 μm. However, no significant effect of film thickness can be observed.

After pore size, pore shape and orientation were evaluated. Elongated pores are anisometric. If they are oriented along a specific direction, they induce anisotropy in the material (if not, the material remains isotropic). Pore orientation was determined by cumulating pore length lying in a defined angle range. In order to differentiate pores with similar lengths but different degrees of anisometry, the pore length was multiplied by its aspect ratio (giving a higher weight to pores that are more elliptical). Finally, the results were normalized with the maximal measured value. Polar plots for the 3 specimen types at a relative density of 90% are displayed in Fig. 4. For the freely sintered sample, pores seem to be more oriented horizontally Fig. 4a. For the 150 μm thick film, pores are more or less randomly distributed with a slight tendency to alignment in the z-direction Fig. 4b. In contrast to this, they are for the 50 μm thick film Fig. 4c clearly more aligned along the z-axis, which is the thickness direction.

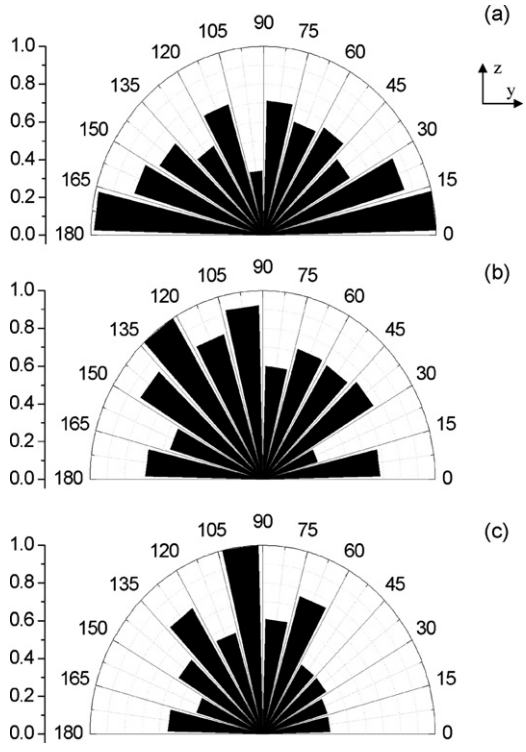

Fig. 4. Cumulated weighted length of pores in the YZ-plane for (a) freely sintered and constrained sintered, (b) 150 μm thick and (c) 50 μm thick films.

In order to quantify the microstructural level of anisotropy, a pore orientation factor was introduced simply defined as the cumulated weighted length measured in the thickness direction (between 75° and 105°) divided by the cumulated weighted length in the *y* direction (between 0° and 15°, as well as between 165° and 180°). This pore orientation factor is equal to 0.53 for the free film, 1.11 for the thicker constrained film and 1.72 for the thinner one, quantifying the fact that the effects of the constraining conditions are more important when the film is thinner. The preferential pore orientation present in free films is certainly induced by the tape casting and lamination steps and may have been more significant in the green state than measured at 90% density, since elongated pores tend to round off if the body sinters freely. In comparison to this reference configuration, a random orientation of the pores as found for the 150 μm thick film signifies an increase of 100% of the pore orientation factor. The constrained films are subjected to pore reorientation perpendicularly to the substrate plane, as already highlighted in ref. 4. Confirming this analysis, the mean pore aspect ratio is found to be equal to 1.85 for the free case, 2.32 for the thicker constrained film and 2.85 for the thinner one, showing that pores are globally more anisometric when the film is constrained and thinner.

3.3. Microstructural gradient through the thickness

A careful observation of the constrained sintered specimens revealed that in the vicinity of the substrate the local density is smaller than the global one and that the microstructure is finer. This constitutes a very thin layer which can be clearly observed in Fig. 5. It is about 3 μm thick, i.e. about 20 grains. Additional snapshots of this area were taken, analysed and showed that at a distance of 2 μm from the substrate the local porosity is 18.9% (compared to 11% for the rest of the film). Pore size distribution is also affected near the substrate as more 0.05–0.1 μm long pores are left than elsewhere. These pores are mostly intergranular and are still interconnected. It is noteworthy that no other zone of higher porosity could be observed elsewhere in the films. It can be concluded that this interface layer is not due to a local binder segregation which after burn-out may lead to a higher porosity and retarded densification[15] but rather to the constraining conditions.

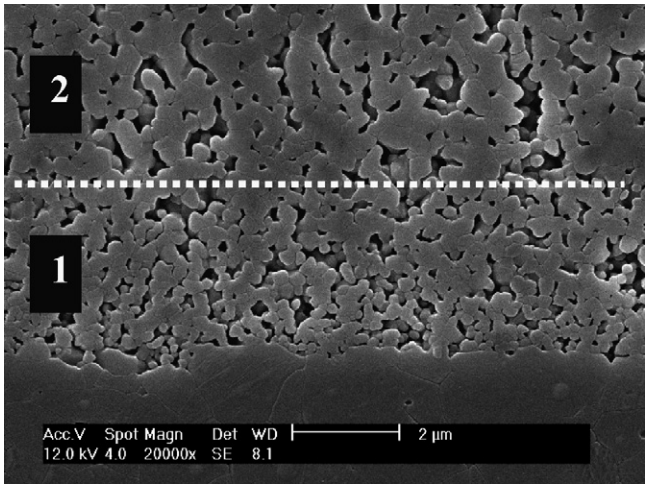

Fig. 5. Polished cross-section of a sintered film showing: (1) interface layer (2) homogeneous film.

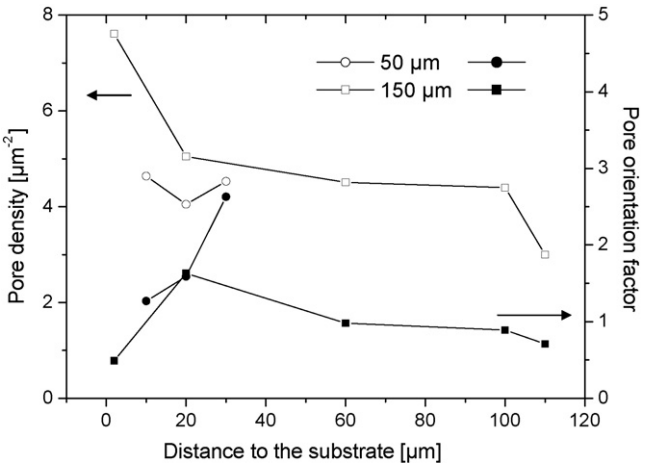

Fig. 6. Pore density and pore orientation factor as a function of the distance to the substrate.

With these additional data, it is possible to plot in Fig. 6 the evolution of the pore density and pore orientation factor along the thickness direction for both constrained films. Final thicknesses are ~35 and 115 μm for the initially 50 and 150 μm thick films. Density hardly changes in this layer between 20 and 100 μm far from the substrate, which could suggest that tensile stress remains almost constant along the thickness direction and that the initial film composition is homogeneous through the thickness. Pore density is higher close to the substrate and decreases slowly up to 10 μm far from the top surface. Underneath the free surface of the thicker film the pore density is smaller. The mean pore size (Feret's diameter) is slightly increasing from 0.26 to 0.31 μm between 20 and 100 μm far from the substrate, which may explain the observed decrease in pore density, as density remains constant along the *z*-axis.

On the other hand, the pore orientation factor changes a lot through the layer thickness. For the thicker film, it starts from 0.49 close to the substrate, increases up to 1.63 at a distance of 20 μm and then decreases slowly down to 0.71 near the free surface. For the thinner film, the pore orientation factor increases continuously from 1.27 at 10 μm from the substrate to 2.63 at a distance of 30 μm (which is also 5 μm underneath the free surface). Apart from this last data point, differences between the two films are relatively small, which let us assume that microstructure may be only dependent on the distance from the substrate and not on the film thickness itself. For example, the pore orientation factor is equal for both films at a distance of 20 μm and pore density are comparable. It seems that the film anisotropy reaches a maximum at about 30–40 μm far from the substrate and then decreases. Pore orientation analysis performed in the interface layer showed that pores are more aligned along the substrate. A possible explanation is that the original configuration of particle packing is maintained near the substrate. The initial microstructure is then preserved as particles cannot rotate. Particle rearrangement, which is an

important process in solid state sintering especially in the early stages of sintering,[16,17] may be hindered during sintering due to friction between alumina particles and alumina substrates at high temperature.

It therefore seems reasonable to define two levels of geometrical constraint. For both of them no lateral shrinkage takes place. For particles which are near the substrate (corresponding to about 20 layers), an additional constraining condition is that particle rearrangement is hindered by the substrate during the initial stage of sintering. This helps to rationalize the macroscopic densification behaviour observed in the first part: the global densification rate is expected to decrease as the ratio of the thicknesses of the interface layer to the total film increases. Apart from this thin interface zone, it seems that the effect of the constraining substrate is hardly dependent on film thickness (which was verified here within an upper limit of about 1000 grains on the top of each other), as long as no delamination or cracking occurs.

In addition, grain morphology was also characterized. As suggested by Bordia and Scherer,[18] necks submitted to compressive or tensile stresses grow at a different rate than if sintered freely. Thus different grain sizes may be encountered in the radial and the hoop direction near a rigid inclusion or substrate plane in the case of constrained thin films. Therefore, the ratio G_y/G_z (G_y and G_z are the grain size in y and z direction) along the thickness direction is plotted in Fig. 7. Once again, curves obtained from both films show a good agreement. The grain size ratio is almost constant (about 1.20) from 20 μm to the top surface of the films and shows a larger value in the vicinity of the substrate (1.40). However, this increase is thought to be the result of the initial particle orientation,[19] as no grain growth took place in the interface layer (density of 80%) which preserves original particle anisometry. Grains are globally a bit more elongated in plane (as a comparison, the mean grain size ratio is 1.05 for a free film densified up to 90%), but we may expect a clearer modification of the grain morphology for higher densities.

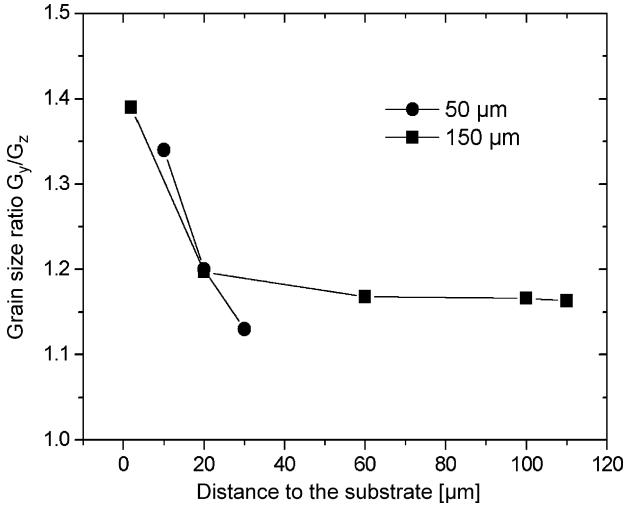

Fig. 7. Grain size ratio as a function of the distance to the substrate.

4. Conclusion

The objective of this work was to better characterize thin film sintering as a function of film thickness, by means of macroscopic shrinkage measurements and microstructure evaluation.

Anisotropy developed clearly in constrained films. Densification retardation and preferential pore orientation were found to be more important for thinner films. The anisotropic effects are nevertheless smaller for grains than for pores. In the vicinity of the substrate a lower density and finer microstructure were observed. The presence of this interface layer is suggested to result from hindered particle rearrangement.

Acknowledgement

This work was financed by the Deutsche Forschungsgemeinschaft (DFG) under Contract No. Ro954/14.

References

1. Bordia, R. K. and Jagota, A., Crack growth and damage in constrained sintering films. *J. Am. Ceram. Soc.*, 1993, **76**(10), 2475–2485.
2. Garino, T. J. and Bowen, H. K., Kinetics of constrained-film sintering. *J. Am. Ceram. Soc.*, 1990, **73**(2), 251–257.
3. Choe, J. W., Calata, J. N. and Lu, G. Q., Constrained-film sintering of a gold circuit paste. *J. Mater. Res.*, 1995, **10**(4), 986–994.
4. Guillon, O., Weiler, L. and Rödel, J., Anisotropic microstructural development during the constrained sintering of dip-coated alumina thin films. *J. Am. Ceram. Soc.*, in press.
5. Scherer, G. W., Viscous sintering on a rigid substrate. *J. Am. Ceram. Soc.*, 1985, **68**(4), 216–220.
6. Bordia, R. K. and Scherer, G. W., On constrained sintering-1. Constitutive model for a sintering body. *Acta Metall.*, 1988, **36**(9), 2393–2397.
7. Bordia, R. K. and Scherer, G. W., On constrained sintering-II. Comparison of constitutive models. *Acta Metall.*, 1988, **36**(9), 2399–2409.
8. Mistler, R. E., Tape casting: the basic process for meeting the needs of the electronics industry. *Am. Ceram. Soc. Bull.*, 1990, **69**(6), 1022–1026.
9. Moreno, R., The role of slip additives in tape-casting technology: part I—solvents and dispersants. *Am. Ceram. Soc. Bull.*, 1992, **71**(10), 1521–1531.
10. Moreno, R., The role of slip additives in tape-casting technology: part II—binders and plasticizers. *Am. Ceram. Soc. Bull.*, 1992, **71**(10), 1647–1657.
11. Frank, M., Jonas, S., Steuer, M., Papenfuhs, B., Besendörfer, G. and Roosen, A., PVB als Binder für das Foliengießen auf der Basis organischer Lösemittel. *Fortschrittsberichte der Deutsche Keramische Gesellschaft*, 2004, **18**(1), 69–74.
12. Guillon, O., Aulbach, E., Bordia, R. K. and Rödel, J., Constrained sintering of alumina thin films: comparison between experiment and modelling. *J. Am. Ceram. Soc.*, submitted for publication.
13. Raj, P. M. and Cannon, W. R., Anisotropic shrinkage in tape-cast alumina: role of processing parameters and particle shape. *J. Am. Ceram. Soc.*, 1999, **82**(10), 2619–2625.
14. Sung, J. S., Koo, K. D. and Park, J. H., Lamination and sintering shrinkage behavior in multilayered ceramics. *J. Am. Ceram. Soc.*, 1999, **82**(3), 537–544.
15. Jean, J. H. and Wang, H. R., Organic distributions in dried alumina green tape. *J. Am. Ceram. Soc.*, 2001, **84**(2), 267–272.
16. Petzow, G. and Exner, H. E., Particle rearrangement in solid-state sintering. *Zeitschrift für Metallkunde*, 1976, **67**(9), 611–618.
17. Weiser, M. W. and de Jonghe, L. C., Rearrangement during sintering in two-dimensional arrays. *J. Am. Ceram. Soc.*, 1986, **69**(11), 822–826.
18. Bordia, R. K. and Scherer, G. W., On constrained sintering-III. Rigid inclusions. *Acta Metall.*, 1988, **36**(9), 2411–2416.
19. Raj, P. M., Odulena, A. and Cannon, W. R., Anisotropic shrinkage during sintering of particle-oriented systems—numerical simulation and experimental studies. *Acta Mater.*, 2002, **50**, 2559–2570.